INTERNATIONAL JOURNAL FOR NUMERICAL AND ANALYTICAL METHODS IN GEOMECHANICS
Int. J. Numer. Anal. Meth. Geomech. 2016; **40**:1383–1401
Published online 14 January 2016 in Wiley Online Library (wileyonlinelibrary.com). DOI: 10.1002/nag.2481

Coupled bonded particle and lattice Boltzmann method for modelling fluid–solid interaction

Min Wang, Y.T. Feng*,† and C.Y. Wang

Zienkiewicz Centre for Computational Engineering, College of Engineering, Swansea University, Swansea SA2 8PP, U.K.

SUMMARY

This paper presents a two-dimensional coupled bonded particle and lattice Boltzmann method (BPLBM) developed to simulate the fluid–solid interactions in geomechanics. In this new technique, the bonded particle model is employed to describe the inter-particle movement and forces, and the bond between a pair of contacting particles is assumed to be broken when the tensile force or tangential force reaches a certain critical value. As a result the fracture process can be delineated based on the present model for the solid phase comprising particles, such as rocks and cohesive soils. In the meantime, the fluid phase is modelled by using the LBM, and the immersed moving boundary scheme is utilized to characterize the fluid–solid interactions. Based on the novel technique case studies have been conducted, which show that the coupled BPLBM enjoys substantially improved accuracy and enlarged range of applicability in characterizing the mechanics responses of the fluid–solid systems. Indeed such a new technique is promising for a wide range of application in soil erosion in Geotechnical Engineering, sand production phenomenon in Petroleum Engineering, fracture flow in Mining Engineering and fracture process in a variety of engineering disciplines. Copyright © 2016 John Wiley & Sons, Ltd.

Received 25 January 2015; Revised 5 September 2015; Accepted 4 November 2015

KEY WORDS: bonded particle model; lattice Boltzmann method; immersed boundary; discrete element method; fluid–solid interaction

1. INTRODUCTION

Dynamics of particle–fluid systems has attracted considerable attention from the community of computational mechanics. The current interest is because of its broad range of applications in petroleum engineering, geotechnical engineering, chemical engineering and biomechanical engineering. In solving the problems the complexity of particle–fluid interactions remains a major challenge that cannot be easily resolved via experiments with high cost and limited resolution. As a result computational simulation has been employed as an alternative technique in characterizing the coupling between solid mechanics and fluid dynamics.

In dealing with fluid dynamics, conventional finite element and finite volume methods face a great challenge in modelling the movement and interaction of particles in fluid. Thus, efforts have been made to develop more efficient numerical techniques in the last two decades. So far, there have been two most commonly used techniques, i.e. (i) a coupled discrete element and computational fluid dynamics method (DEM-CFD) and (ii) a coupled discrete element and lattice Boltzmann method (DEM–LBM). The latter will be discussed in details in the present study.

In early 1990s, the coupled DEM-CFD approach was first proposed by Tsuji *et al.* [1] to investigate fluidized bed in chemical engineering. In this model, a particle (whose size normally is smaller than a

*Correspondence to: Y. T. Feng, Zienkiewicz Centre for Computational Engineering, College of Engineering, Swansea University, Swansea SA2 8PP, U.K.
†E-mail: Y.Feng@Swansea.ac.uk

fluid grid) has two types of motion: translation and rotation. These motions of individual particles are determined by Newton's second law of motion while the overall continuum fluid field is controlled by the continuity condition and the Navier–Stokes (N–S) equations where the local mean variables over a computational cell are used [2–4]. For the problems considering the particle of size larger than one grid, geometrically adapted new meshes have to be used in the model for the fluid in the vicinity of particles. However, if there are too many particles in a system, the problem will become much more complicated for the coupled DEM-CFD approach as the presence of neighbouring particles reduces the space for fluid, generates a high fluid velocity gradient and, finally, yields an increased shear stress on particle surface [5]. To resolve these issues, Hu [6] proposed a direct numerical simulation (DNS) technique, i.e. a fine resolution of CFD for fluid flow, where the fluid field is resolved at a scale comparable with the particle spacing and the particles are treated as discrete moving boundaries. It is found that DNS is able to predict the hydrodynamic interactions between the fluid and particles with highly improved accuracy [5]. On the other hand, as this technique requires to continuously generate geometrically adapted meshes to circumvent severe mesh distortion, this is obviously too computationally intensive, particularly for three-dimensional modelling. Thus its efficiency needs to be further enhanced.

Considering problems encountered in DEM-CFD, Cook *et al.* [7] developed the coupled DEM–LBM technique to resolve the fluid–particle systems. The technique has been validated through a couple of two-dimensional simulations. In this approach, the discrete element method (DEM) is adopted to trace the motions of solid particles. The LBM is utilized to model a fluid flow by tracking the development of distribution functions of molecular assemblies [8–10]. In addition, the immersed boundary scheme [11] was adopted to handle the interaction between moving particles and the fluid [7, 11, 12], and the large eddy simulation (LES) based turbulence model was incorporated into DEM–LBM to improve the accuracy of the simulation in the turbulent fluid flow [13]. Later, this initially two-dimensional (2D) technique was further extended to a three-dimensional (3D) one and validated through a simplified laboratory model [14–16]. The method enjoys highly improved efficiency in handling the fluid–particle issues as it possesses the fine resolution at grain level. In addition, DEM–LBM is naturally paralleled in numerical analyses. Previous studies showed that DEM–LBM can find a wide range of applications in various engineering disciplines [17–24]. Nevertheless, geomaterials are commonly comprised of bonded particles where cohesive forces play an important role in determining their mechanical characteristics. Therefore the bonded particle method (BPM) [25] considering the cohesion forces between bonded particles should be more practical than DEM in simulating the geomaterials such as rocks, soils and concrete.

This work aims to largely improve the accuracy in simulating fluid–particle systems by coupling the BPM and LBM (BPLBM). This novel technique can be particularly useful for the simulations of, e.g. shale oil exploitation process and hydraulic fracture in horizontal directional drilling. Key computational issues, including the algorithm of BPM and the fluid–solid coupling, will be addressed in detail. Actually, BPLBM is an extension of DEM–LBM, not only can it better simulate the mechanical response of geomaterials where cohesion forces exist between bonded particles, but also tackle interactions between granular particles and the fluid. In addition, BPLBM is a mesoscopic or microscopic method, which can process fluid–particle issues at the grain-level commonly ranging from hundreds of microns to several centimetres. Both BPM and LBM are natural to parallelize as their collision process is local. As a result, BPLBM turns out to be even more promising for modelling large-scale even field problems.

In the next section a brief introduction of BPM is given, which is followed by the elaboration of the LBM and the coupling of BPM and LBM. Then, some numerical experiments including the soil erosion and fracture process for the assessment of the coupled BPLBM are performed. Finally, it ends with conclusions and future work on how to improve this coupling method.

2. COMPUTATIONAL METHODOLOGY

In this section, we shall introduce the framework of the coupled BPLBM. In this method, the solid comprising bonded particles or granular particles is modelled by BPM in which the cohesion forces

DOI: 10.1002/nag

between bonded particles are considered by the contact bond model [25] and the fluid flow is solved using LBM with incorporation of the turbulence model. In addition, the fluid–solid interactions are achieved through the immersed moving boundary (IMB) scheme [11] which is commonly used in DEM–LBM.

2.1. Bonded particle method

It has been noted that the bonds existing between adjacent particles can resist both traction and shear forces and will break because of excessive traction and/or shear forces [26, 27]. Therefore, the bonds play a vital role in determining the critical strength and force–displacement behaviour of geomaterials. Nowadays BPM is being extensively used for simulating construction materials i.e. soil, rock and concrete. The concept of BPM is first proposed for rock by Potyondy and Cundall [25]. It originates from the DEM which has been proved to be an effective numerical tool for modelling problems consisting of granular particles. In BPM, the bond model mimicking cementation can be implemented between the particles in contact, and the bonds are able to carry normal forces, tangential forces and moment. When the bond force exceeds its critical value, the contact bond will break. In this case, only the particle–particle contact forces (independent of the bond) need to be considered.

The BPM code used in this work is developed from our in-house DEM program at Swansea University. The treatment of interactions between particles is similar to that in the DEM [28, 29] in which particle–particle interactions are treated as a transient problem where equilibrium state is reached when the internal forces are balanced. The Newton's second law is utilized to determine the translation and rotation of each particle arising from the contact forces, e.g. externally applied forces and body forces as well as cohesive forces, while the force–displacement law is used to update the contact forces that keep changing because of the relative motion of particles at each contact. The dynamic behaviour is represented numerically by a time-stepping algorithm in which the velocities and accelerations are assumed to be constant within each time step. Because the propagation speed of disturbances is a function of the physical properties of the discrete medium, a sufficiently small time step should be chosen so that, in one time step, disturbances cannot propagate from a particle farther than its neighbouring particles. Therefore, at all times the resultant forces on any particle are determined exclusively by the neighbouring particles in contact.

The Newton's second law governing the motion of a particle is given by

$$\mathrm{m}a + \mathrm{c}v = F_c + F_f + \mathrm{m}g \tag{1}$$

$$I\ddot{\theta} = T_c + T_f \tag{2}$$

where m and I are respectively the mass and the moment of inertia of particles, c is a damping coefficient, a and $\ddot{\theta}$ are acceleration and angular acceleration, F_c and T_c are, respectively, contact forces and corresponding torques, and F_f and T_f are hydrodynamic forces and their torques. It should be emphasized that F_c can be either particle–particle contact forces for granular particles or cohesion forces F_b existing between bonded particles.

2.1.1. The particle–particle contact model. The particle–particle contact force F_c has two components, the normal contact force and tangential contact force (see Figure 1), and they are, respectively, given by

Normal interaction laws:

$$F_n = \mathrm{K}_n \delta^{\mathrm{m}} \tag{3}$$

Coulomb friction model:

$$F_t = -\frac{\dot{\delta}_t}{\left|\dot{\delta}_t\right|} \begin{cases} K_t|\delta_t|; & |K_t\delta_t| \le \mu F_n \\ \mu F_n; & |K_t\delta_t| > \mu F_n \end{cases} \tag{4}$$

DOI: 10.1002/nag

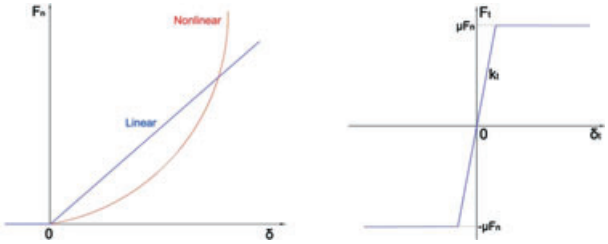

a. Normal contact b. Tangential contact

Figure 1. Particle–particle contact models.

where K_n and K_t are normal stiffness and tangential stiffness, δ_t and $\dot{\delta}_t$ correspond to accumulated tangential sliding and sliding velocity, δ is the overlap of two particles. The coefficient m can be 1 and 3/2, the former is for the linear contact and the latter is for the Hertz contact model.

2.1.2. The contact bond model. The bond model used this work is referred to as the contact bond model [25, 30]. It approximates the physical behaviour of a vanishingly small cemented-like substance joining the two bonded particles. It can be envisioned as a pair of elastic springs (or a point of glue) with constant and shear stiffness acting at the contact point. These two springs have specified shear and tensile strength. The existence of a contact bond precludes the possibility of slip. This widely accepted bond model accounts for forces acting at the contact point, but it is unable to describe a moment applied. Thus more advanced bond model is required to simulate more complicated mechanical behaviours [25, 31].

The contact bond is characterized by two parameters, i.e. normal bond strength (F_{bn}) and shear bond strength (F_{bs}). If the tensile contact force equals or exceeds the normal contact bond strength, the bond breaks, and both the normal and shear contact forces are set to be zero. Differently, when the shear contact force is equal or greater than the shear contact bond strength, the bond breaks, but the contact forces do not change. The contact bond model shown in Figure 2 can be described by
Normal component:

$$F_n^b = \begin{cases} K_n^b \delta; & F_n^b \le F_{\max} \\ 0; & F_n^b > F_{\max} \end{cases} \tag{5}$$

Tangential component:

$$F_t^b = -\frac{\dot{\delta}_t}{|\dot{\delta}_t|} \begin{cases} K_t^b |\delta_t|; & |K_t^b \delta_t| \le \mu F_n^b \\ \mu F_n^b; & |K_t^b \delta_t| > \mu F_n^b \end{cases} \tag{6}$$

where K_n^b and K_t^b are the normal stiffness and tangential stiffness for the cement, $F_{\max}$ is the critical tensile force.

2.1.3. The selection of time step. As mentioned before, the DEM is based upon the idea that the time step chosen is so small that disturbances cannot propagate from any disc further than its

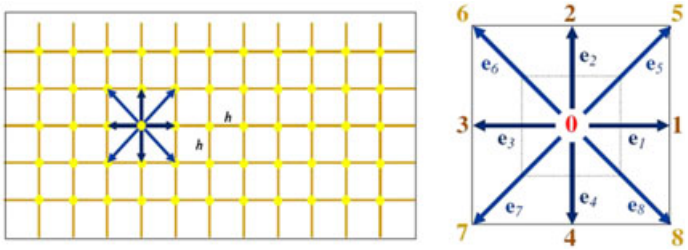

Figure 2. LB discretization and D2Q9 model: (a) a standard LB lattice and (b) D2Q9 model.

DOI: 10.1002/nag

immediate neighbours during one single time step. Currently, the critical time step can be determined by two methods based on a linear dynamic system and wave propagation, respectively. The former is valid for a linear system and can be obtained by the formulae below without considering damping forces [29, 32]

$$t_{crit} = 2\sqrt{m/k}\ (\text{Single mass} - \text{spring system}) \tag{7}$$

$$t_{crit} = \begin{cases} \sqrt{m/k} & Translation \\ \sqrt{I/k^{rot}} & Rotation \end{cases} (\text{Multiple mass} - \text{spring system}) \tag{8}$$

where K^{rot} is the rotational stiffness.

By examining the cases of uniform circular and spherical particles with regular packing configurations, O'Sullivan and Bray [33] proposed that a smaller critical time step $t_{crit} = 0.17\sqrt{m/k}$ is more appropriate for three-dimensional DEM simulations involving uniform-sized particles and $t_{crit} = 0.3\sqrt{m/k}$ should be used for the two-dimensional DEM simulations involving uniform-sized disks.

The critical time step based on wave propagation can be determined by wave speed and the diameter of the smallest particle [34].

$$t_{crit} = \frac{\pi R_{ave}}{\eta}\sqrt{\frac{\rho_s}{G}} \tag{9}$$

$$\eta = 0.8766 + 0.1631v \tag{10}$$

where R_{ave}, ρ_s, ν, and G are the average radius, density, Poisson's ratio and shear modulus of the particles, respectively.

Given the damping forces [35], the critical time step can be obtained by

$$t_{crit} = 2\sqrt{m/k}\left(\sqrt{1+\xi^2} - \xi\right)(\text{Single mass} - \text{spring system}) \tag{11}$$

where $\xi = c/\left(2\sqrt{km}\right)$, or

$$t_{crit} = \sqrt{m/k}\left(\sqrt{1+\xi^2} - \xi\right)(\text{Multiple mass} - \text{spring system}) \tag{12}$$

with $\xi = c/\left(4\sqrt{km}\right)$.

In determining the critical time steps we should consider the time steps in both normal direction and shear direction and the smaller one is used as the critical time step that is controlled by the smallest particle.

In the consideration of both accuracy and stability, the time step used in DEM simulations is taken as

$$\Delta t = \lambda \cdot t_{crit} \tag{13}$$

where the time step factor λ is typically chosen to be 0.1– 0.2.

In this study the critical time step is calculated by Eq. 12.

2.1.4. The general algorithm of BPM. A brief introduction to the computational procedures of the BPM is given as follows:

DOI: 10.1002/nag

1. A particle packing with a specified size distribution will be generated first. Then, the first contact detection will be performed to build up a contact list for bonded particles and install bond models into bonded particles;
2. Relax the sample until the balance state is reached. After that, the boundary conditions will be applied for the first time-step calculation;
3. Carry out the global contact detection and work out the overlap between contact particles for the subsequent contact force calculation;
4. Then check whether these contact pairs are on the bond contact list, if yes, use the contact bond model to calculate the cohesion forces between bonded particles, otherwise calculate contact forces between no bonded pairs using the particle–particle contact models;
5. Check the calculated bond forces, if the tensile force or shear force exceeds its critical value, remove these contact pairs from the bond contact list;
6. Use Newton's Second law to update the position and velocity of each particle;
7. Repeat Steps 3–6 till the specific time interval is exceeded and output the useful data for postprocess.

The principal issues in BPM are the calculation of contact forces and the contact detection. The processing of contact forces has been introduced in this paper. Detailed discussion of contact detection algorithms can be found in the literatures [36, 37]. Considering the efficiency in terms of CPU and memory, we used the NBS [37, 38] contact detection algorithm in this work.

2.2. Lattice Boltzmann method

The LBM is a microscopic or mesoscopic approach for fluid dynamics analysis. The primary variables of LBM are fluid density distribution functions instead of pressure and velocity considered in the conventional CFD. In LBM, the fluid domain is divided into regular lattices. The fluid phase is treated as a group of (imaginary) fluid particles which are allowed to move to the adjacent lattice nodes or stay at rest. During each discrete time step, fluid particles at individual lattice nodes move to their immediate neighbouring lattice nodes along the given directions. Thus, at each node, collision occurs between the fluid particles from the neighbouring nodes. The macro fluid behaviour can be described through the statistics of the motion of fluid particles. The governing equation in LBM is the lattice Boltzmann (LB) equation. Its counterpart in conventional CFD is the well-known N–S equation. In particular, the N–S equation can be recovered from the LB equation under the condition of low Mach number [39].

The LBM is originated from lattice gas automata (LGA) developed to eliminate the statistical noise. The first LB model is called the MZ model [40], where the density distribution functions instead of Boolean variables were employed for particle treatment. It was then simplified to the HJ model by Higuera and Jiménez [41] through linearizing the collision operator. The technique, however, suffers from poor numerical stability. To solve the problem, the HSB model was proposed [42]. Because the collision operator in the HSB model is out of the collision rule in LGA, the technique is deemed as a great progress in the model development. Two years later, the Bhatnagar–Gross–Krook (BGK) model was proposed to simplify the collision operator in the HSB model, and it is a single relaxation model as only one relaxation parameter is introduced in collision process [39, 43]. Subsequently, the multiple-relaxation- time (MRT) model was developed where multiple relaxation parameters are introduced [44]. The MRT model is better than BGK model in terms of calculation accuracy and stability but its computing is higher.

2.2.1. Bhatnagar–Gross–Krook (BGK) model. Given the computational efficiency and ease in programming, the BGK model is adopted in this work. It can be characterised by the following LB equation:

$$f_i(x + e_i\Delta t, t + \Delta t) - f_i(x, t) = \Omega \tag{14}$$

where f_i is the primary variables in the LB formulation (so-called fluid density distribution functions), and Ω is the collision operator. In the BGK model, Ω is characterised by a relaxation time τ and the equilibrium distribution function $f_i^{eq}(x, t)$

DOI: 10.1002/nag

$$\Omega = -\frac{\Delta t}{\tau}[f_i(x,t) - f_i^{eq}(x,t)]. \tag{15}$$

To make further explanation about LBM, we will take the widely used 2D LB discretization scheme, the so-called D2Q9 model, as an example.

The fluid domain is discretized into square lattices with side h. Particles at each node are allowed to move to its eight immediate neighbours with different velocities e_i (i = 1,2,..,8). A proportion of the particles can rest at the node with a zero velocity e_0. As shown in Figure 2(b), the nine discrete velocity vectors in total are defined as

$$e_0 = (0,0),$$

$$e_i = C\left(cos\frac{\pi(i-1)}{2}, sin\frac{\pi(i-1)}{2}\right) \quad (i = 1,\ldots,4), \tag{16}$$

$$e_i = C\left(cos\frac{\pi(2i-9)}{4}, sin\frac{\pi(2i-9)}{4}\right) \quad (i = 5,\ldots,8).$$

Here C is the lattice speed and is related to lattice side, h, and time step, Δt

$$C = h/\Delta t.$$

The central issue to LBM is to control the movement of fluid particles via the density distribution functions. The evolution of the density distribution functions at each time step is governed by Equation 14. The equilibrium distribution function can be defined as

$$f_i^{eq} = \omega_i\rho\left(1 + \frac{3}{C^2}e_i\cdot v + \frac{9}{2C^4}(e_i\cdot v)^2 - \frac{3}{2C^2}v\cdot v\right) \quad (i = 0,\ldots,8) \tag{17}$$

where ρ and v are the macroscopic fluid density and velocity, respectively and ω_i are the weighting factors:

$$\omega_0 = \frac{4}{9}, \quad \omega_{1,2,3,4} = \frac{1}{9}, \quad \omega_{5,6,7,8} = \frac{1}{36}. \tag{18}$$

The macroscopic fluid density ρ and velocity v can be calculated from the distribution functions

$$\rho = \sum_{i=0}^{8} f_i, \quad \rho v = \sum_{i=1}^{8} f_i e_i. \tag{19}$$

The fluid pressure is given by

$$P = C_S^2\rho \tag{20}$$

where C_S is termed the fluid speed of sound and is related to the lattice speed C

DOI: 10.1002/nag

$$C_S = C/\sqrt{3}. \tag{21}$$

The kinematic viscosity, υ, of the fluid is implicitly determined by

$$\upsilon = \frac{1}{3}\left(\tau - \frac{1}{2}\right)\frac{h^2}{\Delta t} = \frac{1}{3}\left(\tau - \frac{1}{2}\right)Ch \tag{22}$$

2.2.2. Turbulence modelling. Although LBM has been proved to be efficient for a variety of fluid flow with low Reynolds number, not much work has been done on the modelling of turbulent flow using LBM except a previous study [45]. However, the turbulent flow is common in engineering problems, and it is one of the most active research topics in CFD.

LES is a well-known turbulence modelling approach in the engineering field, which enables one to directly solve large spatial-scale turbulent eddies that carry the majority of the energy. The smaller-scale eddies are described by using a subgrid model. The separation of these scales is achieved through filtering the N–S equations, from which solutions to the resolved scales are obtained. In this study, the widely used one-parameter Smagorinsky subgrid model [46] is adopted, where the Reynolds stress tensor is assumed to be dependent only on the local strain rate.

A simple route to incorporate turbulence model is to directly apply the concept of LES to the LB formulation [45]. Following this approach, the filtered form of the LB equation is expressed as

$$\widetilde{f}_i(x + e_i\Delta t, t + \Delta t) - \widetilde{f}_i(x,t) = -\frac{1}{\tau_*}\left[\widetilde{f}_{\mathrm{i}}(x,t) - \widetilde{f}_i^{eq}(x,t)\right] \tag{23}$$

where $\widetilde{f}_i$ and $\widetilde{f}_i^{eq}$ represent the distribution function and the equilibrium distribution function of the resolved scales, respectively. The effect of the unresolved scale motion is modelled through an effective collision relaxation time scale τ_{t}. Thus the total relaxation time τ_* is described by

$$\tau_* = \tau + \tau_{\mathrm{t}} \tag{24}$$

where τ and τ_{t} are the relaxation times corresponding to the fluid viscosity υ and the turbulence viscosity υ_{t}, respectively. Accordingly, υ_* is given by

$$\upsilon_* = \upsilon + \upsilon_t = \frac{1}{3}\left(\tau_* - \frac{1}{2}\right)\frac{h^2}{\Delta t} = \frac{1}{3}\left(\tau + \tau_{\mathrm{t}} - \frac{1}{2}\right)C^2\Delta t \tag{25}$$

$$\upsilon_t = \frac{1}{3}\tau_t C^2 \Delta t \tag{26}$$

where the turbulence viscosity υ_{t} is calculated in terms of the filtered strain rate tensor $\widetilde{\mathrm{S}}_{\mathrm{ij}}$ and a filter length scale h

$$\upsilon_t = (S_c h)^2 \widehat{S}, \tag{27}$$

$$\widehat{S} = \frac{\widehat{Q}}{2\rho C_S^2 \tau_*}. \tag{28}$$

In which $\mathrm{S_c}$ is the Smagorinsky constant, $\hat{\mathrm{S}}$ the characteristic value of the filtered strain rate tensor $\widetilde{\mathrm{S}}_{\mathrm{ij}}$ and $\widehat{\mathrm{Q}}$ the filtered mean momentum flux can be computed from second-order moments $\widetilde{\mathrm{Q}}_{\mathrm{ij}}$, with

DOI: 10.1002/nag

$$\widehat{S} = \sqrt{\sum_{i,j} \widetilde{S}_{ij}\widetilde{S}_{ij}}; \quad \widehat{Q} = \sqrt{2\sum_{i,j} \widetilde{Q}_{ij}\widetilde{Q}_{ij}}.$$

Consequently, the turbulence relaxation time τ_t is obtained as

$$\tau_t = \frac{1}{2}\left(\sqrt{\tau^2 + 18(S_C h)^2 (\rho C^4 \Delta t)^{-1} \widehat{Q}} - \tau\right). \tag{29}$$

This extended LBM including turbulent flows is simple to implement and has been proved promising for turbulence simulations [45] and was first introduced into the DEM–LBM in [13].

2.3. *The fluid–solid interactions*

The fluid–solid interaction is a primary issue in the fluid–particle systems especially when a large number of particles are involved. In order to correctly model the fluid–solid interaction, the no-slip condition must be satisfied, in which the fluid and solid should have the same velocity at the fluid–solid interface. For a stationary particle, this no-slip condition can be easily imposed by the well-known bounce-back rule.

2.3.1. Link-bounce-back rules for stationary particles and moving particles. The link-bounce-back boundary condition [13, 22, 47–49] is straightforward to implement by representing the solid using lattice nodes. Figure 3 shows the lattice discretization of a particle in fluid, where nodes interior and exterior to the particle are the solid and fluid nodes, respectively. A link lies between the solid and fluid nodes, and a boundary node is set in the middle of the link. The surface of the solid is assumed to be located at the boundary node. The lattice nodes on either side of the boundary surface are treated in an identical fashion. The bounce-back rule is applied at boundary node so that the incoming fluid components from fluid nodes are reflected back.

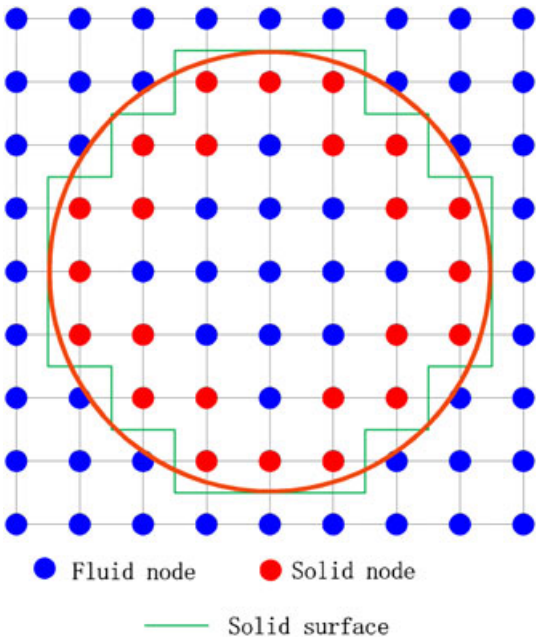

Figure 3. Lattice representation of a circular solid particle.

DOI: 10.1002/nag

$$f_{-i}(x, t + \Delta t) = f_i^{+}(x, t) \tag{30}$$

where f_i^+ represents the density distribution after collision, -i is the opposite direction of i.

Modifications were proposed to the original bounce-back rule by Ladd [48] so that the movement of a solid particle can be accommodated. Although this method can guarantee momentum conservation, not surprisingly, it results in a stepwise representation of the surface of a circular particle, which is neither accurate nor smooth unless small enough lattice spacing is used. Furthermore, with the movement of the particle the boundary nodes will continually change, but in an on–off way. This will cause oscillation to the hydrodynamic forces [13].

2.3.2. Immersed boundary method (IBM). The immersed boundary method is first proposed by Peskin [50]. The basic idea of the IBM is to treat the particle boundary as deformable body with high stiffness. The moving boundaries are represented by a set of boundary nodes. A small distortion of the particle boundary caused by the fluid–particle interactions will generate a force that tends to restore the particle into its original shape. The deformation is calculated by comparing the boundary point and the reference point that undergoes rigid body motions with particles. Then, the N–S equations are solved over the whole fluid–particles domain. This approach has been widely used in CFD [51].

The IBM was introduced to the LBM by Feng and Michaelides [52]. The N–S equation is replaced by the LB equation including an external force f

$$f_i(x + e_i\Delta t, t + \Delta t) - f_i(x, t) = -\frac{\Delta t}{\tau}[f_i(x, t) - f_i^{eq}(x, t)] + \frac{3}{2}\omega_i f \cdot e_i. \tag{31}$$

The no-slip condition at the fluid–particle interfaces is satisfied by calculating the velocity of particle boundary points through the interpolation of the fluid velocities on neighbouring nodes. After calculating the hydraulic force at each boundary points, the body force f will be obtained by

$$F_i = -\kappa\xi_i \tag{32}$$

where F_i and ξ_i are the hydraulic force applied to the i^{th} boundary point of the particle and its corresponding deformation, respectively; and κ is a spring constant. Finally the hydraulic force applied to the particle can be obtained by the summation of the force at each boundary point.

2.3.3. Immersed moving boundary (IMB). In order to solve the problems in the modified bounce-back rule for moving particles, Noble and Torczynski [11] proposed a new boundary scheme (see Figure 4).

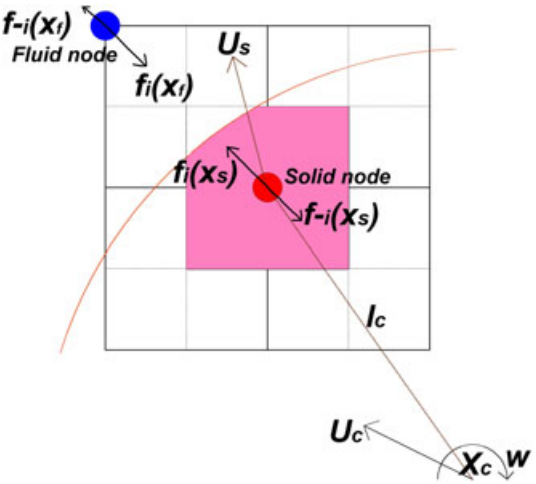

Figure 4. Immersed moving boundary scheme.

DOI: 10.1002/nag

This is accomplished by introducing an additional collision term, Ω_i^S, for nodes covered partially or fully by the solid. Then the collision term in the LB equation including the body force becomes

$$\Omega = -\frac{\Delta t}{\tau}(1-B)[f_i(x,t) - f_i^{eq}(x,t)] + (1-B)\Delta t F_i + B\Omega_i^S \tag{33}$$

where B is a weighting function that depends on the local solid ratio ε, defined as the fraction of the node area (see Figure 8):

$$B = \frac{\varepsilon(\tau - 0.5)}{(1-\varepsilon) + (\tau - 0.5)} \tag{34}$$

when $\varepsilon = 0$, B = 0; $\varepsilon = 1$, B = 1.

The additional collision term is based on the bounce-rule for nonequilibrium part and is given by

$$\Omega_i^S = f_{-i}(x,t) - f_i(x,t) + f_i^{eq}(\rho, U_S) - f_{-i}^{eq}(\rho, u) \tag{35}$$

where U_S is the velocity of the solid node at time step $t + \Delta t$.

$$U_S = U_C + \omega \times l_C \quad \left(l_C = \sqrt{(x - x_C)^2 + (y - y_C)^2}\right) \tag{36}$$

The resultant hydrodynamic force and torque exerted on the solid can be calculated by

$$F_f = Ch\left[\sum_n \left(B_n \sum_i \Omega_i^s e_i\right)\right], \tag{37}$$

$$T_f = Ch\{\sum_n \left[(x - x_C) \times \left(B_n \sum_i \Omega_i^s e_i)\right]\right\}. \tag{38}$$

Later this method was modified by Holdych [53]. The modified version is as follows

$$\Omega_i^S = f_{-i}(x,t) - f_i(x,t) + f_i^{eq}(\rho, U_S) - f_{-i}^{eq}(\rho, U_S). \tag{39}$$

The only difference is that the solid velocity is used to calculate the equilibrium distribution for the last term. The modified IMB was validated and proved to be better in calculating the hydrodynamic forces [16, 21]. In addition, this scheme can recover the classic bounce-back rule for stationary particles; while at B = 0 it reduces to the standard LB equation. However, it seems that there is a non-convergence problem with the modified IMB scheme in our study.

2.3.4. Validation of fluid–solid coupling scheme (IMB). In order to examine the feasibility of the IMB scheme used in this work, the extensively used one single particle sedimentation in fluid was carried out. In our simulation (see Figure 5), a water-filled tube in 2-cm diameter (X-direction) and 6-cm height (Y-direction) is used. The fluid domain is divided into 200×600 square lattices with spacing h = 0.1 mm. The kinematic viscosity and density of fluid are $1.0 \times 10^{-6}\,\mathrm{m^{2/s}}$ and $1000\,\mathrm{kg/m^3}$, respectively. The density of the solid particle is $3000\,\mathrm{kg/m^3}$, and its radius is 0.125 cm. Four boundaries of this simulation are stationary walls and thus the no-slip boundary condition is imposed. Initially, the particle is positioned at (1 cm, 4 cm) with the static state. Because of gravity force, the particle will fall down. The immersed moving boundary scheme is employed to resolving the particle–fluid interaction. To demonstrate the accuracy of IMB, the same simulation using the implicit velocity correction based IBM [54] instead of IMB scheme is carried out. The evolution of particle velocity and hydrodynamic forces applied to the particle with respect to time are compared in Figures 6, 7.

DOI: 10.1002/nag

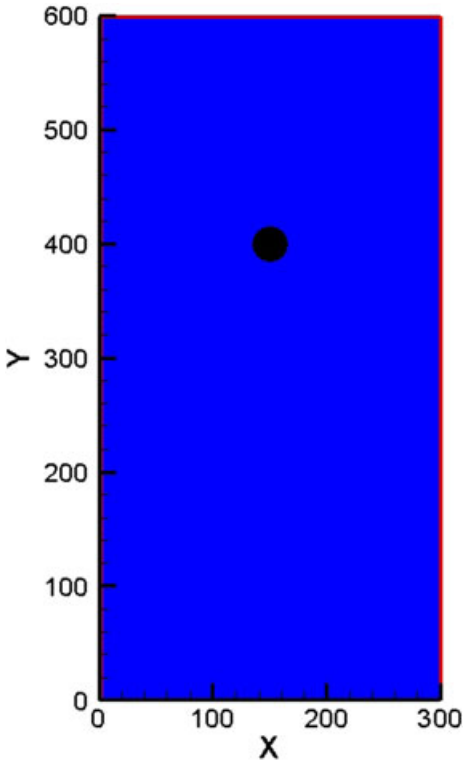

Figure 5. Particle sedimentation model.

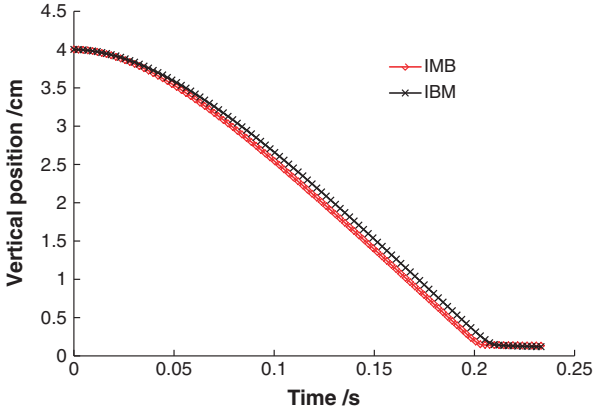

Figure 6. Comparison of particle movement in Y direction.

We can find that the motions of the particle simulated by two IMB and IBM schemes match very well. At the beginning, the particle falls down as an accelerated motion because of gravity force. After a distance it will move with a constant speed as the gravity force, hydrodynamic force and buoyancy reach equilibrium state. It is noticed that the hydrodynamic force calculated by IMB evolves smoothly except one point where the particle collides the bottom boundary. While, the drag forces obtained from IB scheme fluctuate around those calculated by IMB with the development of time.

Since the 1990s considerable effort has been made to study the fluid-moving boundary interaction [55–57]. Because of the accuracy and computational stability of the IMB, the original IMB technique [7, 12–14, 18, 20, 47, 58] has been widely used in DEM–LBM coupling and is adopted in this study.

DOI: 10.1002/nag

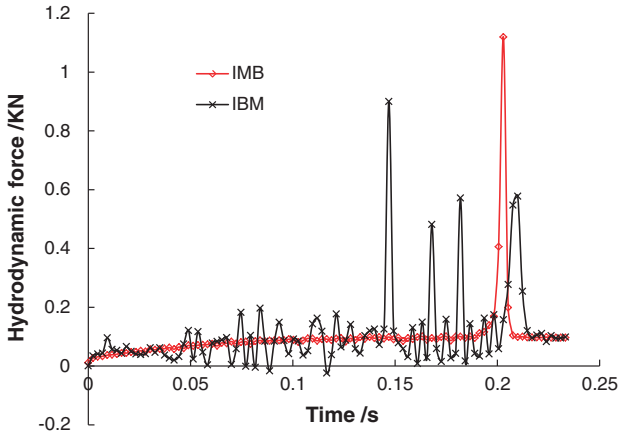

Figure 7. Comparison of drag forces applied to particle.

3. RESULTS AND DISCUSSIONS

In this section, two numerical tests are carried out to demonstrate the efficiency of the coupled bonded particle and LBM (BPLBM). The two problems considered are, respectively, a soil erosion phenomenon under the suction pump and a hydraulic fracture process in the construction of underground tunnel. For comparison, each case is simulated by both DEM–LBM and BPLBM. In the latter method, cohesion or bond forces are considered and the effect of bonds on the mechanic behaviour of the geomaterials can be explored.

In 2D simulation by combining DEM and other fluid method, like CFD and LBM, there is big issue in pore water flow path. Because the flow paths are always blocked up by contacted spheres, it is difficult to obtain realistic flow channels. In order to solve this problem, Boutt *et al.* [17] proposed a method in which the radius of the particle will be reduced to certain degree (called effective radius) artificially when the fluid flow is implemented. This effective hydraulic radius can be accomplished by introducing a ratio of effective radius to the particle radius.

3.1. Case 1—Soil erosion under a suction force

In this case we try to simulate the transport of particles along a suction pipe (see Figure 8). Two simulations of soil samples with cohesion and without cohesion forces are conducted and compared with each other. The setup of the model is given in Figure 8. The size is 0.1 m × 0.1 m and 273 particles of different sizes are considered. The fluid domain is divided into 200 × 200 lattices with spacing h = 0.5 mm. The parameters of the fluid and solid particles are tabulated in Table I. In addition, constant pressure boundary conditions are imposed at the bottom ($\rho_{in} = 1000$ kg/m^3) and the outlet ($\rho_{out} = 999$ kg/m^3). The other boundaries are solid walls.

The snapshots of the evolution process are given in Figure 9 where the erosion process is captured through the BPLBM technique for both granular soils and cohesive soils. Erosion can be seen only in granular sands and the particles are gradually washed away along the suction pipe one by one; while no particles are absorbed up in cohesive soils and the bonded particles move as a whole because of cohesion forces between bonded particles. The difference between the two soils is apparent during the whole process. Natural soils are commonly cohesive and can be hardly treated as granular material using DEM. The BPM is suitable for geomaterials and the couple BPLBM is promising for modelling the fluid–soil interactions in geotechnical engineering. The study of bond parameters will be beneficial to the migration of soil liquefaction.

3.2. Case 2—Hydraulic fracture process in tunnelling

Case 2 simulates a hydraulic fracture process triggered by the horizontal directional drilling in underground construction. The model with sides 0.1 m × 0.1 m is shown in Figure 10 and it is comprised of 488 bonded particles of different sizes (see Figure 11b). The fluid domain is divided

DOI: 10.1002/nag

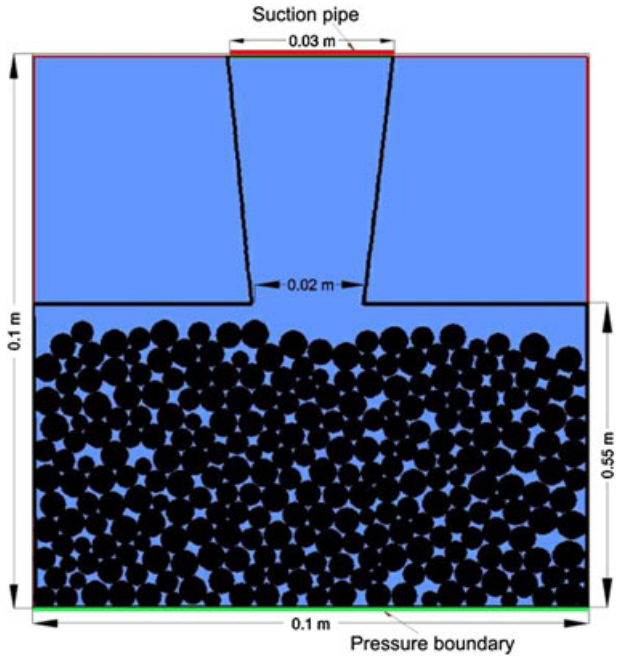

Figure 8. Case 1—soil erosion under a suction force: problem setup.

Table I. Parameters for the fluid and solid.

Parameter	Value	Parameter	Value
Particle density (kg/m^3)	3000	Fluid density (kg/m^3)	1000
Friction coefficient	0.3	Kinematic viscosity (υ)	1.0×10^6
Particle contact stiffness (N/m)	5.0×10^7	Bond contact stiffness (N/m)	2.0×10^7
Bond strength (N)	3000	Smagorinsky constant (S_c)	0.1
Contact damping ratio (ξ)	0.5	Time-step factor (λ)	0.1

into 200×200 lattices with spacing $h=0.5$ mm. The parameters of the fluid and solid particles are the same in the previous erosion simulation. A pressure pipe ($\rho_{in}=1005$ kg/m^3) is applied in the middle of the left vertical wall. At the right boundary, a solid wall which is only effective for solid particles and a pressure boundary ($\rho_{out}=1000$ kg/m^3) for the fluid are implemented. The other boundaries are stationary walls. At the meantime, a corresponding numerical test with 488 granular particles is conducted for comparison.

Figure 11 gives the states of simulation at several different time steps. It can be found that the onset of fracture is captured in Figure 11b, which is achieved by breaking the bond model between particles undergoing too large forces. At the beginning small cavity is formed near the pressure pipe. Then a horizontal hydraulic fracture is formed because of high fluid pressure. With the progress of excavation, the hydraulic fracture grows gradually. In the granular soil test, a cavity is easily formed and it grows up quickly. Finally, a big hole can be seen near the pipe and no fracture appears. The bond effect is apparent through the comparison of the simulations with and without the bond model. The preliminary result demonstrates that this coupled BPLBM is promising for hydraulic fracture study in shale oil exploitation where the experiments and conventional numerical methods have limited resolutions.

In the above two test cases, the calculated lattice speed is the same $C=600$ m/s, while the maximum physical fluid velocities are respectively $v_{max}=0.27$ m/s and $v_{max}=1.44$ m/s. Therefore, the maximum Mach number and Reynolds number can be calculated from the following equations

$$Ma=\frac{v_{max}}{C}, \tag{40}$$

DOI: 10.1002/nag

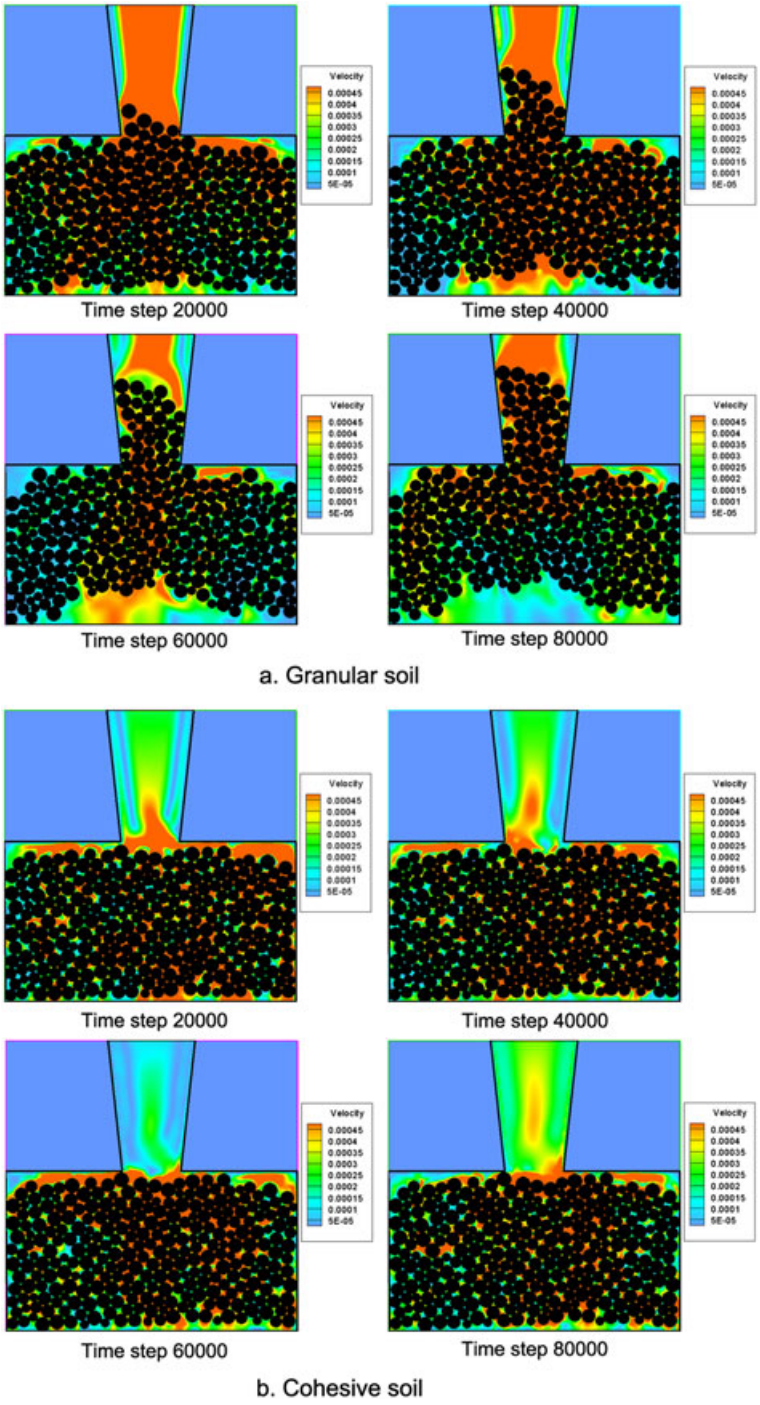

Figure 9. Lattice velocity contour of soil erosion without (a) and with (b) bonds.

$$Re = \frac{v_{max} L}{\upsilon}. \tag{41}$$

The calculated maximum Mach numbers for the soil erosion and hydraulic fracture cases are, respectively, 4.5×10^{-4} and 2.4×10^{-3}. The Mach numbers indicate that the fluid simulation is reasonably accurate, as they are much smaller than 1. The corresponding Reynolds numbers are 1080 and 5760.

DOI: 10.1002/nag

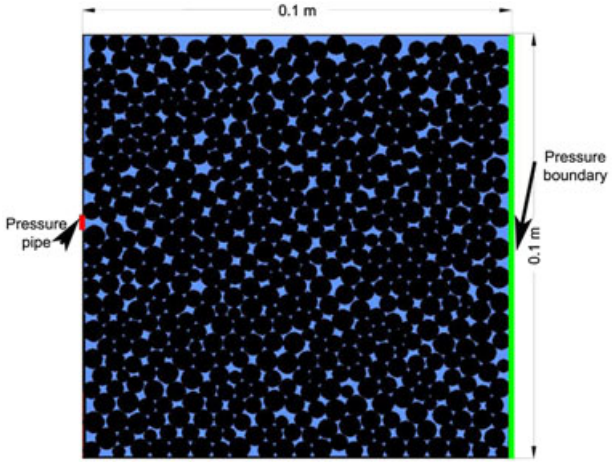

Figure 10. Case 2—hydraulic fracture: problem setup.

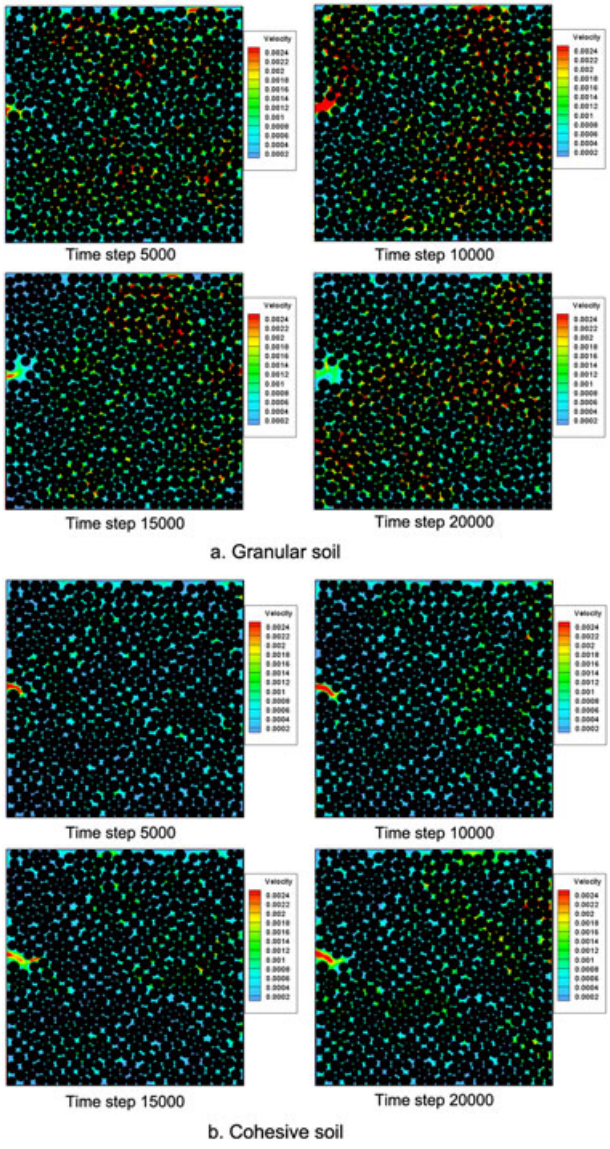

Figure 11. Lattice velocity contour of hydraulic fracture without (a) and with (b) bonds.

DOI: 10.1002/nag

4. CONCLUSIONS

This paper introduces a coupled BPLBM for the simulation of fluid–solid interactions in fluid–particle systems. Numerical tests confirm that the coupled BPLBM technique is promising and efficient in handling problems of soil erosion and hydraulic fracture. Compared to DEM–LBM, it enjoys substantially improved accuracy and enlarged range of applicability in characterizing the mechanics responses of geomaterials in which cohesion forces play an important role. Furthermore, BPLBM is a mesoscopic or microscopic method, which can process fluid–particle issues at the grain-level which commonly ranges from hundreds of microns to several centimetres. This characteristic is difficult to achieve in continuum method. Because of the explicit time-stepping scheme and nature to parallelize, BPLBM is promising for modelling large-scale even field problems using parallel computing.

The present work only presents a 2D BPLBM technique, but the extension of 2D to 3D would be straightforward. Although only a simple bond model has been incorporated in BPLBM, advanced bond models able to resist moment will be developed and validated experimentally in the near future.

REFERENCES

1. Tsuji Y, Tanaka T, Ishida T. Lagrangian numerical simulation of plug flow of cohesionless particles in a horizontal pipe. *Powder Technology* 1992; **71**:239–250.
2. Hoomans BPB, Kuipers J a M, Briels WJ, Van Swaaij WPM. Discrete particle simulation of bubble and slug formation in a two-dimensional gas-fluidised bed: a hard-sphere approach. *Chemical Engineering Science* 1996; **51**:99–118.
3. Tsuji Y, Kawaguchi T, Tanaka T. Discrete particle simulation of two-dimensional fluidized bed. *Powder Technology* 1993; **77**:79–87.
4. Xu BH, Yu AB. Numerical simulation of the gas-solid flow in a fluidized bed by combining discrete particle method with computational fluid dynamics. *Chemical Engineering Science* 1997; **52**:2785–2809.
5. Zhu HP, Zhou ZY, Yang RY, Yu AB. Discrete particle simulation of particulate systems: theoretical developments. *Chemical Engineering Science* 2007; **62**:3378–3396.
6. Hu HH. Direct simulation of flows of solid–liquid mixtures. *International Journal of Multiphase Flow* 1996; **22**:335–352.
7. Cook B. K., Noble, D. R., Preece, D. S., Williams, J. R. Direct simulation of particle-laden fluids. *In Pacific Rocks 2000*, Girard, J., Liebman, M., Breeds, C. *and* Doe, T. (eds), Balkema: Rotterdam. 2000, 279–286.
8. Guo Z., Zheng, C., Li, Q., Wang, N. 2002. Lattice Boltzmann method for hydrodynamics. (In Chinese).
9. Satofuka N, Nishioka T. Parallelization of lattice Boltzmann method for incompressible flow computations. *Computational Mechanics* 1999; **23**:164–171.
10. Succi S. *The Lattice Boltzmann Equation for Fluid Dynamics and Beyond*. Oxford University Press: Oxford, 2001.
11. Noble DR, Torczynski JR. *A Lattice-Boltzmann Method for Partially Saturated Computational Cells*. World Scientific: Singapore, 1998; 1189–1201.
12. Cook BK, Noble DR, Williams JR. A direct simulation method for particle–fluid systems. *Engineering Computations* 2004; **21**:151–168.
13. Feng YT, Han K, Owen DRJ. Coupled lattice Boltzmann method and discrete element modelling of particle transport in turbulent fluid flows: computational issues. *International Journal for Numerical Methods in Engineering* 2007; **72**:1111–1134.
14. Feng YT, Han K, Owen DRJ. Combined three-dimensional lattice Boltzmann method and discrete element method for modelling fluid–particle interactions with experimental assessment. *International Journal for Numerical Methods in Engineering* 2010; **81**:229–245.
15. Owen DRJ, Leonardi CR, Feng YT. An efficient framework for fluid–structure interaction using the lattice Boltzmann method and immersed moving boundaries. *International Journal for Numerical Methods in Engineering* 2011; **87**:66–95.
16. Strack OE, Cook BK. Three-dimensional immersed boundary conditions for moving solids in the lattice-Boltzmann method. *International Journal for Numerical Methods in Fluids* 2007; **55**:103–125.
17. Boutt DF, Cook BK, Mcpherson BJOL, Williams JR. Direct simulation of fluid–solid mechanics in porous media using the discrete element and lattice-Boltzmann methods. *Journal of Geophysical Research* 2007; **112**.
18. Cui X, Li J, Chan A, Chapman D. A 2D DEM–LBM study on soil behaviour due to locally injected fluid. *Particuology* 2012; **10**:242–252.
19. Delenne J-Y, Mansouri M, Radjaï F, Youssoufi MSE, Seridi A. Onset of immersed granular avalanches by DEM–LBM approach. In *Advances in Bifurcation and Degradation in Geomaterials*, Bonelli S, Dascalu C, Nicot F (eds.). Springer Netherlands, 2011.
20. Han Y, Cundall PA. LBM–DEM modeling of fluid–solid interaction in porous media. *International Journal for Numerical and Analytical Methods in Geomechanics* 2013; **37**:1391–1407.

DOI: 10.1002/nag

21. Jones, B. Characterisation of porous media using the Lattice Boltzmann method. *Ph.D. thesis*, *Swansea University*. 2013.
22. Mansouri M, Delenne JY, El Youssoufi MS, Seridi A. A 3D DEM–LBM approach for the assessment of the quick condition for sands. *Comptes Rendus Mecanique* 2009; **337**:675–681.
23. Mansouri M, Delenne JY, Seridi A, El Youssoufi MS. Numerical model for the computation of permeability of a cemented granular material. *Powder Technology* 2011; **208**:532–536.
24. Wang Y, Xue S, Xie J. *A Fully Coupled Solid and Fluid Model for Simulating Coal and Gas Outburst with DEM and LBM*. 2013.
25. Potyondy DO, Cundall PA. A bonded-particle model for rock. *International Journal of Rock Mechanics and Mining Sciences* 2004; **41**:1329–1364.
26. Delenne J-Y, El Youssoufi MS, Cherblanc F, Bénet J-C. Mechanical behaviour and failure of cohesive granular materials. *International Journal for Numerical and Analytical Methods in Geomechanics* 2004; **28**:1577–1594.
27. Jiang MJ, Sun YG, Li LQ, Zhu HH. Contact behavior of idealized granules bonded in two different interparticle distances: an experimental investigation. *Mechanics of Materials* 2012; **55**:15.
28. Cundall P. A., Strack, O. D. L. The distinct element method as a tool for research in granular media. *Report to the National Science Foundation Concerning NSF Grant ENG76-20711*, 1978.
29. Cundall PA, Strack ODL. A discrete numerical model for granular assemblies. *Geotechnique* 1979; **29**:47–65.
30. Itasca Consulting Group Inc. Particle flow code in 2 dimensions. *version 3.0*. *Minnesota*, *U.S.A*. 2002.
31. Potyondy DO. Simulating stress corrosion with a bonded-particle model for rock. *International Journal of Rock Mechanics and Mining Sciences* 2007; **44**:677–691.
32. Itasca Consulting Group Inc. Particle flow code in 3 dimensions. *version 4.0*. *Minnesota*, *U.S.A*. 2010.
33. O'sullivan C, Bray JD. Selecting a suitable time step for discrete element simulations that use the central difference time integration scheme. *Engineering Computations* 2004; **21**:278–303.
34. Thornton C, Randall CW. Applications of theoretical contact mechanics to solid particle system simulation. In *Micromechanics of Granular Materials, Satake and Jenkins (eds)*. Elsevier Science Publishers: Amsterdam, Netherlands, 1988; 133–142.
35. Feng YT. On the central difference algorithm in discrete element modelling of impact. *International Journal for Numerical Methods in Engineering* 2005; **64**:1959–1980.
36. Feng YT, Owen DRJ. An augmented spatial digital tree algorithm for contact detection in computational mechanics. *International Journal for Numerical Methods in Engineering* 2002; **55**:159–176.
37. Munjiza, A. The combined finite-discrete element method. London. 2004.
38. Munjiza A, Andrews KRF. NBS contact detection algorithm for bodies of similar size. *International Journal for Numerical Methods in Engineering* 1998; **43**:131–149.
39. Chen H, Chen S, Matthaeus WH. Recovery of the Navier–Stokes equations using a lattice-gas Boltzmann method. *Physical Review A* 1992; **45**:5339–5342.
40. Mcnamara GR, Zanetti G. Use of the Boltzmann equation to simulate lattice-gas automata. *Physical Review Letters* 1988; **61**:2332–2335.
41. Higuera FJ, Jiménez J. Boltzmann approach to lattice gas simulations. *EPL (Europhysics Letters)* 1989; **9**:663–668.
42. Higuera FJ, Succi S, Benzi R. Lattice gas dynamics with enhanced collisions. *EPL (Europhysics Letters)* 1989; **9**:345–349.
43. Chen S, Chen H, Martinez DO, Matthaeus WH. Lattice Boltzmann model for simulation of magnetohydrodynamics. *Physical Reviews Letters* 1991; **67**:3776–3779.
44. D'humieres D, Ginzburg I, Krafczyk M, Lallemand P, Luo LS. Multiple-relaxation-time lattice Boltzmann models in three dimensions. *Philosophical Transactions of the Royal Society A: Mathematical, Physical and Engineering Sciences* 2002; **360**:437–451.
45. Huidan Y, Girimaji SS, Li-Shi L. DNS and LES of decaying isotropic turbulence with and without frame rotation using lattice Boltzmann method. *Journal of Computational Physics* 2005; **209**:599–616.
46. Smagorinsky J. General circulation experiments with the primitive equations. *Monthly Weather Review* 1963; **91**:99–164.
47. Han K, Feng YT, Owen DRJ. Coupled lattice Boltzmann and discrete element modelling of fluid–particle interaction problems. *Computers and Structures* 2007; **85**:1080–1088.
48. Ladd AJC. Numerical simulations of particulate suspensions via a discretized Boltzmann equation. Part 1. Theoretical foundation. *Journal of Fluid Mechanics* 1994; **271**:285–309.
49. Ladd AJC, Verberg R. Lattice-Boltzmann simulations of particle–fluid suspensions. *Journal of Statistical Physics* 2001; **104**:1191–1251.
50. Peskin CS. Numerical analysis of blood flow in the heart. *Journal of Computational Physics* 1977; **25**:220–252.
51. Peskin CS. The immersed boundary method. *Acta Numerica* 2002; **11**:479–517.
52. Feng ZG, Michaelides EE. The immersed boundary-lattice Boltzmann method for solving fluid–particles interaction problems. *Journal of Computational Physics* 2004; **195**:602–28.
53. Holdych D. J. Lattice Boltzmann methods for diffuse and mobile interfaces. University of Illinois at Urbana, 2003.
54. Dash SM, Lee TS, Lim TT, Huang H. A flexible forcing three dimension IB–LBM scheme for flow past stationary and moving spheres. *Computers & Fluids* 2014; **95**:159–170.
55. Aidun CK, Lu Y, Ding EJ. Direct analysis of particulate suspensions with inertia using the discrete Boltzmann equation. *Journal of Fluid Mechanics* 1998; **373**:287–311.

DOI: 10.1002/nag

56. Kao PH, Yang RJ. An investigation into curved and moving boundary treatments in the lattice Boltzmann method. *Journal of Computational Physics* 2008; **227**:5671–5690.
57. Lallemand P, Luo L-S. Lattice Boltzmann method for moving boundaries. *Journal of Computational Physics* 2003; **184**:406–421.
58. Han Y, Cundall PA. Lattice Boltzmann modeling of pore-scale fluid flow through idealized porous media. *International Journal for Numerical Methods in Fluids* 2011; **67**:1720–1734.

DOI: 10.1002/nag